IEEJ Journal of Industry Applications
Vol.7 No.1 pp.49–55 DOI: 10.1541/ieejjia.7.49

**Paper**

# Design Optimization Method for the Load Impedance to Maximize the Output Power in Dual Transmitting Resonator Wireless Power Transfer System

Takahiro Koyama[*a)] Student Member, Kazuhiro Umetani[*] Member
Eiji Hiraki[*] Member

(Manuscript received Jan. 25, 2017, revised June 11, 2017)

Recently, the dual transmitting resonator wireless power transfer system (DTR-WPT) has been proposed as a promising technique for the power supply of mobile apparatus. Although this technique has been reported to be effective for increasing the output power as well as for covering a wide area during wireless power transfer, the complicated magnetic coupling among two transmitting resonators and one receiving resonator makes it difficult to develop practical design optimization methods, thus hindering practical applications of this technique. The purpose of this paper is to propose a design optimization method for the load impedance of DTR-WPT. This method is derived based on a novel simple equivalent circuit model of the DTR-WPT. The optimum impedance derived using this method as well as the appropriateness of the equivalent circuit were verified experimentally, thus validating usefulness of the proposed method for the practical application of DTR-WPT.

**Keywords:** dual transmitting resonators, magnetic coupling, wireless power transfer, load impedance

## 1. Introduction

Recently, resonant inductive coupling wireless power transfer [(1)–(9)] (WPT) is attracting growing attention as a convenient electric power supply method. In literature, there have been proposed a number of applications of resonant inductive coupling WPT to various apparatus, such as laptops [(10)], biomedical implants [(11)–(14)], and electric vehicles [(15)–(19)].

Particularly, application of WPT to small mobile apparatus, such as mobile phones and laptops, is emerging as a promising field of techniques. The WPT technique may be utilized for power supply to these apparatus disposed or moving in wide space. This may remove the limit of the operating time that has been caused by the charge capacity of the battery. Furthermore, the battery itself may even be eliminated by continuously supplying the power using the WPT technique. However, the WPT to small mobile apparatus in wide space often suffers from low power transfer capability, particularly when the apparatus is at a distant place from the transmitting resonator. Therefore, the WPT is intensely required to improve the power transfer capability to a distant place.

One reason of this difficulty may lie in the composition of a typical resonant inductive coupling WPT system. A typical WPT system consists of one transmitting resonator and one receiving resonator [(1)–(19)], as presented in Fig. 1(a). Hereafter, we refer to it as the single transmitting resonator (STR-WPT) system. The power transfer of the STR-WPT system is dependent on the magnetic coupling between the transmitting and receiving resonators. However, the coupling

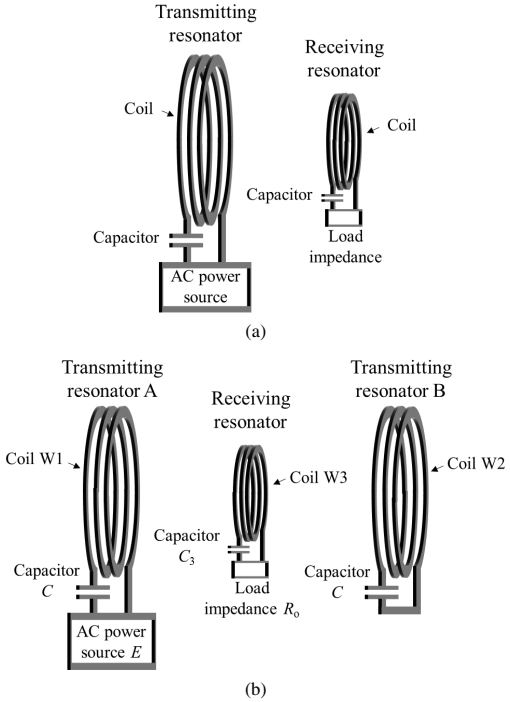


Fig. 1. Single transmitting resonator wireless power transfer (STR-WPT) system (a) and dual transmitting resonators (DTR) wireless power transfer system (b)

a) Correspondence to: Takahiro Koyama. E-mail: pk430kpd@s.okayama-u.ac.jp
* Graduate School of Natural Science and Technology, Okayama University
3-1-1, Tsushimanaka, Kita-ku, Okayama 700-8530, Japan

© 2018 The Institute of Electrical Engineers of Japan.

coefficient becomes weak as the distance between the transmitting and receiving resonators becomes large, thus decreasing the power transfer capability to a distant place.

In order to mitigate this difficulty, the dual transmitting resonator WPT (DTR-WPT) has been proposed in a preceding work [20]. Figure 1(b) illustrates the DTR-WPT system. The DTR-WPT system consists of two transmitting resonators and one receiving resonator, which is sandwiched by the transmitting resonators. One transmitting resonator A is connected to an AC power source. On the other hand, the other transmitting resonator B is a LC resonator without any load nor power source. The coils of the transmitting resonators are designed to have sufficient size so that magnetic coupling between these resonators can excites large resonance in transmitting resonator B. As a result, both of these transmitting resonators can transfer the power to the receiving resonator.

In DTR-WPT, the receiving resonator can be disposed in wide space between the two transmitting resonators. Therefore, transmitting resonator B can transfer the power to the receiving resonator, even if the receiving resonator moves at a distant place from transmitting resonator A. As a consequence, DTR-WPT can offer higher power transfer capability in wider space than STR-WPT.

Certainly, a number of previous studies [21][22] have proposed WPT systems with multiple transmitting resonators disposed at a long distance. In these systems, all the transmitting resonators are designed to have the AC power source. However, this may cause inconvenience because the resonators may require their own AC power sources. Otherwise, the resonators may require long wire to share the AC power source, deteriorating the Q factor of the resonators. On the other hand, the DTR-WPT system does not need to connect transmitting resonator B to the AC power source. Therefore, the DTR-WPT system may be convenient for practical applications.

In spite of this attractive feature of the DTR-WPT system, operation analysis of this system tends to be difficult because of complex magnetic coupling among the three resonators. This difficulty may hinder elucidation of the design optimization methods for the DTR-WPT system.

The purpose of this paper is to derive a design optimization method of the load impedance for the DTR-WPT system. This paper focuses the load impedance because this impedance may be comparatively easily optimized by the electric power conversion circuits, such as DC-DC converters, switched capacitors, or rectifying circuits. Certainly, the optimization of the transmitting and receiving coils may also significantly contribute to improvement in the performance of the DTR-WPT system. However, design of the coils tends to have limitation of the installation space; and therefore, optimization of the coils is not easily applicable in many cases. On the other hand, the load impedance may be comparatively easily optimized using the small-sized onboard power conversion circuits. Therefore, optimization of the load impedance may be applicable to many practical applications.

In this paper, we define the optimum load impedance as the load impedance that maximizes the output power when the receiving resonator is placed at the center between the two transmitting resonators. As mentioned above, the DTR-WPT system is expected to supply power to small apparatus in wide space between the transmitting resonators. Therefore, the system is required to supply sufficient power to operate the apparatus even if the apparatus is placed at the point of the lowest power transfer capability. In the DTR-WPT system, the power transfer capability is the lowest when the receiving resonator is placed at the center between the two transmitting resonators, because the receiving resonator is distant from both of the transmitting resonators. Therefore, the load impedance is required to maximize the output power at the center point between the transmitting resonators.

Certainly, the output power can be increased infinitely, if there is no limit of the amplitude of the input AC voltage source. However, practical AC voltage source such as voltage-fed inverters generally has a limitation of maximum AC voltage output. Therefore, we discuss maximization of the output power under a given amplitude of the AC voltage source.

This paper analyzes the optimum load impedance based on the equivalent circuit model of the DTR-WPT. For convenience, we assume that the two transmitting resonators are symmetric. The equivalent circuit model is simplified using the standard circuit theory. Then, the optimum load impedance is calculated based on analysis of the simplified equivalent circuit model.

The following discussion consists of four sections. Section 2 presents theoretical derivation of the optimum load impedance. Section 3 presents the experiment to verify the result of section 2. Finally, section 4 gives conclusions.

## 2. Analysis of the Optimum Load Impedance

**2.1 Simplified Equivalent Circuit Model** First, this subsection derives the simplified equivalent circuit model of the DTR-WPT based on the system presented in Fig. 1(b). Transmitting coils W1 and W2 are assumed to have the same self-inductance $L$ and the same parasitic resistance $R$ because W1 and W2 are assumed to be symmetric. The mutual inductance between W1 and W2 is denoted as $M_{TR}$. The mutual inductance between W1 and W3 also equals to $M_{TR}$ because the receiving resonator is placed at the center between two transmitting resonators.

As a result, we can express Fig. 1(b) as the equivalent circuit model shown in Fig. 2. Symbol $E$ is the AC power source; $C$ is the capacitor of transmitting resonators; $M_{TT}$ is mutual inductance between W1 and W2; $r$, $L_3$ and $C_3$ are the parasitic resistance, self-inductance of W3 and the capacitor of receiving resonator, respectively. The number of turns of W1 and W2 is denoted as $n_x$, whereas that of W3 is denoted as $n_y$. Resistance $R_o$ represents the load impedance. Furthermore, $i_1$, $i_2$ and $i_3$ are the current flowing in the transmitting and receiving resonators, respectively; $v_{13}$ and $v_{23}$ are the voltage induced by the mutual inductance between coils W1 and W3 and between coils W2 and W3, respectively.

According to the circuit theory, we can formulate $v_{13}$, $v_{23}$ and $i_3$ as

$$v_{13} = j\omega\frac{n_x}{n_y}M_{TR}\left(i_1 + \frac{n_y}{n_x}i_3\right), \cdots\cdots\cdots\cdots\cdots\cdots (1)$$

$$v_{23} = j\omega\frac{n_x}{n_y}M_{TR}\left(i_2 + \frac{n_y}{n_x}i_3\right), \cdots\cdots\cdots\cdots\cdots\cdots (2)$$

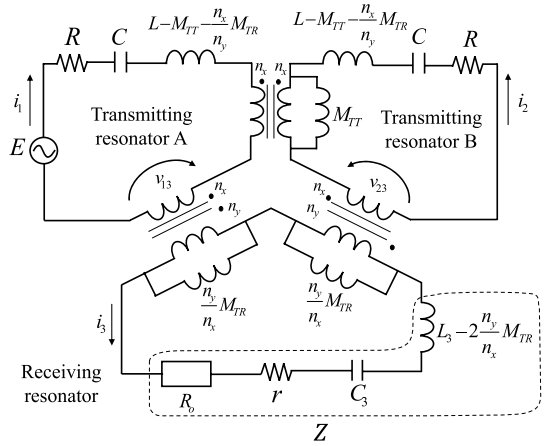


Fig. 2. Basic equivalent circuit model of the DTR-WPT system

$$-Zi_3 = j\omega\frac{n_y}{n_x}M_{TR}\left(\frac{n_x}{n_y}i_1 + i_3\right) + j\omega\frac{n_y}{n_x}M_{TR}\left(\frac{n_x}{n_y}i_2 + i_3\right), \quad \cdots\cdots (3)$$

where $Z$ is the impedance of the subcircuit surrounded by the dashed line in Fig. 2, defined as

$$Z = r + R_o + j\left(\omega L_3 - 2\frac{n_y}{n_x}\omega M_{TR} - \frac{1}{\omega C_3}\right). \cdots\cdots (4)$$

Substituting (3) into (1) and (2) yields

$$v_{13} = \frac{\frac{n_x}{n_y}M_{TR}Z}{\frac{Z}{j\omega} + 2\frac{n_y}{n_x}M_{TR}}i_1 + \frac{j\omega M_{TR}^2}{\frac{Z}{j\omega} + 2\frac{n_y}{n_x}M_{TR}}(i_1 - i_2), \quad \cdots\cdots (5)$$

$$v_{23} = \frac{\frac{n_x}{n_y}M_{TR}Z}{\frac{Z}{j\omega} + 2\frac{n_y}{n_x}M_{TR}}i_2 + \frac{-j\omega M_{TR}^2}{\frac{Z}{j\omega} + 2\frac{n_y}{n_x}M_{TR}}(i_1 - i_2). \quad \cdots\cdots (6)$$

Equation (5) is obtained by eliminating $i_3$ from (1) and (3). On the other hand, (6) is obtained by eliminating $i_3$ from (2) and (3). Based on (5) and (6), the equivalent circuit model that does not contain $i_3$ is obtained as shown in Fig. 3, where impedance $Z_1$, $Z_2$ and $Z_3$ are defined as

$$Z_1 = Z_3 = \frac{\frac{n_x}{n_y}M_{TR}Z}{\frac{Z}{j\omega} + 2\frac{n_y}{n_x}M_{TR}}, \quad \cdots\cdots (7)$$

$$Z_2 = \frac{j\omega M_{TR}^2}{\frac{Z}{j\omega} + 2\frac{n_y}{n_x}M_{TR}}. \quad \cdots\cdots (8)$$

Next, Fig. 3 is transformed into a simplified T-shaped equivalent circuit model. As can be seen in Fig. 3, one transformer has the additive polarity and the other has the subtractive polarity. We transform the latter transformer into a transformer with the additive polarity. As a result, we obtain Fig. 4, in which $Z_1 + 2Z_2$ and $Z_3 + 2Z_2$ are obtained as

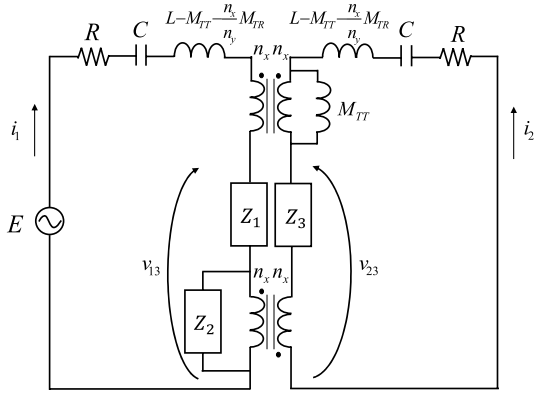

Fig. 3. Modified equivalent circuit model obtained from the basic equivalent circuit shown in Fig. 2

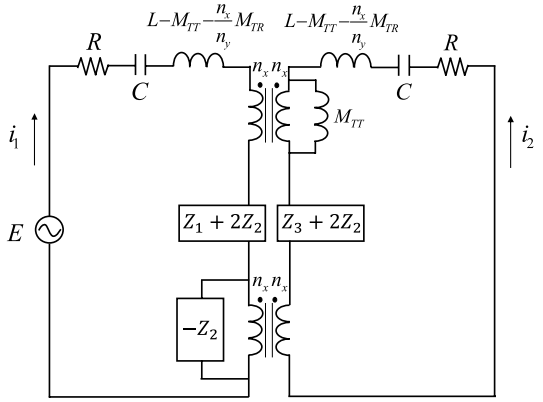

Fig. 4. Equivalent circuit model with two transformers having additive polarity

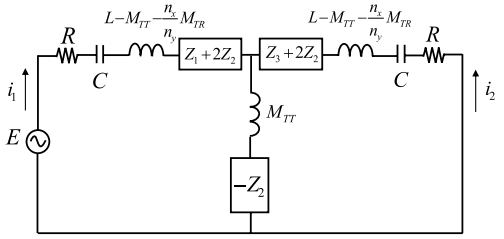

Fig. 5. Equivalent circuit model that replaced the transformers in Fig. 4 by the T-shaped equivalent circuit

$$Z_1 + 2Z_2 = Z_3 + 2Z_2 = \frac{\frac{n_x}{n_y}M_{TR}Z + 2j\omega M_{TR}^2}{\frac{Z}{j\omega} + 2\frac{n_y}{n_x}M_{TR}} = j\omega\frac{n_x}{n_y}M_{TR}. \cdots\cdots (9)$$

The transformers in the equivalent circuit model is integrated into one transformer with the additive polarity. Then, the integrated transformer is replaced by the T-shaped equivalent circuit. As a result, we obtain Fig. 5.

Noticing that $Z_1 + 2Z_2$ and $Z_3 + 2Z_2$ are equivalent to the impedance of the inductance, we can integrate them with the leakage inductance $L - M_{TT} - n_xM_{TR}/n_y$. In addition, we formulate the impedance $-Z_2$ by substituting (4) into (8) and then divide the impedance $-Z_2$ into the real part $R_A$ and the imaginary part $X_A$. As a result, $R_A$ and $X_A$ are expressed as

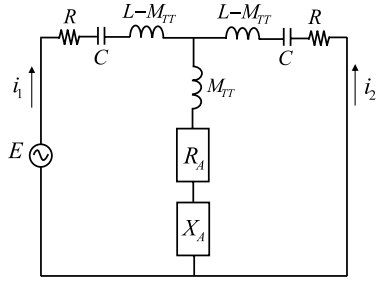


Fig. 6. Simplified equivalent circuit model

$$R_A = \frac{\omega^2 M_{TR}^2 (R_o + r)}{(R_o + r)^2 + \left(\omega L_3 - \frac{1}{\omega C_3}\right)^2}, \quad \cdots\cdots (10)$$

$$X_A = -\frac{\omega^2 M_{TR}^2 \left(\omega L_3 - \frac{1}{\omega C_3}\right)}{(R_o + r)^2 + \left(\omega L_3 - \frac{1}{\omega C_3}\right)^2}. \quad \cdots\cdots (11)$$

Finally, we obtain the simplified equivalent circuit model shown in Fig. 6. In the next subsection, we derive the optimum load impedance based on the analysis of Fig. 6.

**2.2 Optimum Load Impedance** According to Fig. 6, $i_1$ is solved as

$$i_1 = \frac{E}{R + j\left(\omega L - \omega M_{TT} - \frac{1}{\omega C}\right) + Z_g}, \quad \cdots\cdots (12)$$

where $Z_g$ is defined as

$$Z_g = \frac{\left\{R + j\left(\omega L - \omega M_{TT} - \frac{1}{\omega C}\right)\right\}\{R_A + j(X_A + \omega M_{TT})\}}{R + R_A + j\left(X_A + \omega L - \frac{1}{\omega C}\right)}. \quad \cdots\cdots (13)$$

In addition, $i_2$ is solved as

$$i_2 = -\frac{R_A + j(X_A + \omega M_{TT})}{R + R_A + j\left(X_A + \omega L - \frac{1}{\omega C}\right)} i_1. \quad \cdots\cdots (14)$$

Hence, $i_1 + i_2$ is expressed as

$$i_1 + i_2 = \frac{R + j\left(\omega L - \omega M_{TT} - \frac{1}{\omega C}\right)}{R + R_A + j\left(X_A + \omega L - \frac{1}{\omega C}\right)} i_1 \quad \cdots\cdots (15)$$

On the other hand, substituting (3) into (4) yields

$$i_3 = -\frac{j\omega M_{TR}}{R_o + r + j\left(\omega L_3 - \frac{1}{\omega C_3}\right)} (i_1 + i_2), \quad \cdots\cdots (16)$$

Eliminating $i_1$ and $i_2$ from (12), (15) and (16), we can obtain the output power $P(\omega, R_o)$ as

$$P(\omega, R_o) = |i_3|^2 R_o$$

$$= \left| \frac{-\omega^2 M_{TR}^2 E^2}{\left[\{R + j\alpha\}\left\{\sqrt{R_o} + \frac{r + j\beta}{\sqrt{R_o}}\right\} + \frac{2\omega^2 M_{TR}^2}{\sqrt{R_o}}\right]^2} \right|, \quad \cdots\cdots (17)$$

where $\alpha$ and $\beta$ are defined as

$$\alpha = \omega L + \omega M_{TT} - \frac{1}{\omega C}, \quad \cdots\cdots (18)$$

$$\beta = \omega L_3 - \frac{1}{\omega C_3}. \quad \cdots\cdots (19)$$

The optimum load impedance $R_o$ that maximizes $P(\omega, R_o)$ can be obtained as $R_o$ that minimizes the denominator of the right-most side of (17). As a result, the maximum output power $P_{\max}(\omega)$ at given $\omega$ is obtained as

$$P_{\max}(\omega) = \left| \frac{-\omega^2 M_{TR}^2 E^2}{2\sqrt{\gamma} + 2r\alpha^2 + 2R^2 r + 4R\omega^2 M_{TR}^2} \right|, \quad \cdots\cdots (20)$$

where $\gamma$ is defined as

$$\gamma = \left\{\left(Rr + 2\omega^2 M_{TR}^2 - \alpha\beta\right)^2 + (R\beta + r\alpha)^2\right\}\left(R^2 + \alpha^2\right). \quad \cdots\cdots (21)$$

In addition, the load resistance $R_o$ that maximizes $P(\omega, R_o)$ is obtained as

$$R_o = \sqrt{\frac{(Rr + 2\omega^2 M^2 - \alpha\beta)^2 + (R\beta + r\alpha)^2}{R^2 + \alpha^2}}. \quad \cdots\cdots (22)$$

As can be seen in (20), $P_{\max}(\omega)$ is a function of the angular frequency. The angular frequency $\omega$ can be optimized by searching for $\omega$ that maximizes $P_{\max}(\omega)$. Finally, the optimum load resistance at the optimum angular frequency can be obtained by substituting this optimum angular frequency into (22).

## 3. Experiment

Experiment was carried out to verify the simplified equivalent circuit model and the optimum load impedance for maximizing the output power. Figure 7 presents the photographs of the experimental transmitting and receiving coils. Specifications of the experimental transmitting and receiving resonators are presented in Table 1. The small coil was employed for the receiving coil. On the other hand, the large coils were employed for the transmitting coils so that the transmitting resonator A can excite resonance in the transmitting resonator B. All resonators were designed so that the resonance frequency was set at 200 kHz. (The angular frequency was 1.26M rad/s).

Figure 8 presents the disposition of the experimental coils. The receiving coil was disposed at the center between the transmitting coils. The distance between the two transmitting coils was set at 70 mm; and the distance between the transmitting coil and the receiving coil was set at 25 mm. As a result, $M_{TT}$ was measured as 1.63 $\mu$H, whereas $M_{TR}$ was measured as 2.02 $\mu$H.

(a) Transmitting coil (b) Receiving coil

Fig. 7. Experimental transmitting and receiving coils

Table 1. Specifications of the experimental resonators

| | Transmitting resonators | Receiving resonator |
|---|---|---|
| Coil diameter | 70.0mm | 35.0mm |
| Coil width | 53.0mm | 20.0mm |
| Self-inductance | 59.1$\mu$H | 17.0 $\mu$H |
| Capacitance | 9.62nF | 37.5nF |
| Number of turns | 33 | 23 |
| AC Resistance | 0.955 Ω at 200kHz (1.26Mrad/s) | 0.754 Ω at 200kHz (1.26Mrad/s) |

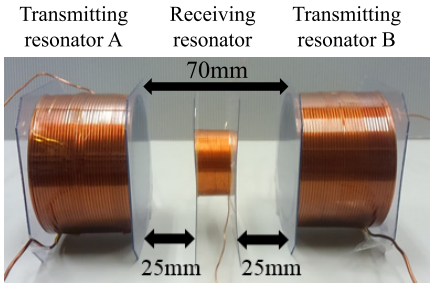


Fig. 8. Disposition of the experimental coils

Table 2. Measurement instruments

| Instrument | Manufacturer | Model |
|---|---|---|
| Oscilloscope | Tektronix | DPO3034 |
| Current probe (Transmitting resonators) | Tektronix | TCP305A |
| Current probe (Receiving resonator) | Tektronix | TCP312 |
| Voltage probe | Tektronix | P6139B |

**3.1 Verification of the Simplified Equivalent Circuit Model** First, we compared the amplitude of the current in the transmitting and receiving coils between the experimental evaluation result and the theoretical prediction based on the simplified equivalent circuit model. In this experiment, we applied the AC voltage with the amplitude of 10.0 Vp-p to the transmitting resonator A. In addition, we set the load resistance at 10 Ω. Table 2 shows the measurement instruments for the experiment.

Figure 9 and Fig. 10 show the comparison result. The solid line is the theoretical prediction based on the analysis of the simplified equivalent circuit model, i.e. (12), (14), and (16). Figure 9 shows the frequency dependency of the experimental and theoretical current amplitude for a wide angular frequency range, whereas Fig. 10 shows the frequency dependency for a narrower angular frequency range near the resonant angular frequency. Because of the limited S/N ratio of the current measurement, too small current value below −55 dBA is not presented in Fig. 9.

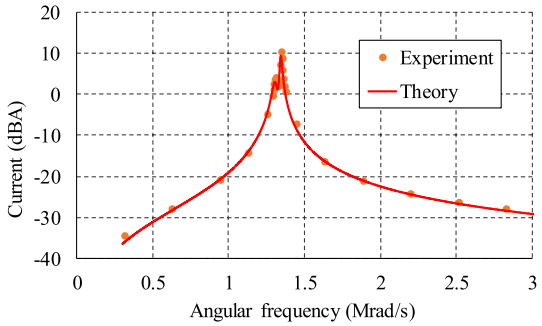


(a) Amplitude of current $i_1$ of transmitting coil W1.

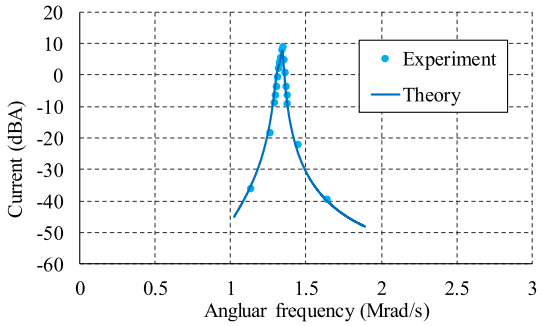


(b) Amplitude of current $i_2$ of transmitting coil W2.

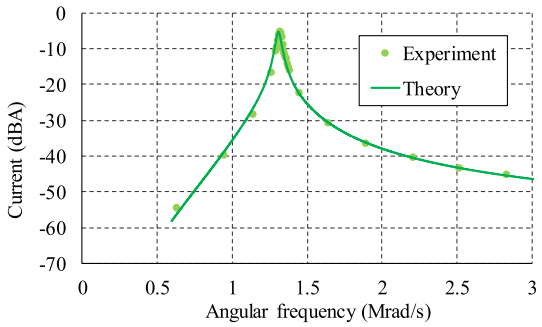


(c) Amplitude of current $i_3$ of receiving coil W3.

Fig. 9. Frequency dependency of experimental current amplitude in the transmitting and receiving coils

As can be seen in Fig. 9 and Fig. 10, experimental results agreed well with the theoretical prediction. Therefore, the experiment supported appropriateness of the simplified equivalent circuit model as well as the analysis result of this circuit.

Figure 10(a) showed two peaks in the frequency dependency of the transmitting resonator current $i_1$. Similarly, the slight depression on the top of the peak in Fig. 10(b) also implies the existence of two peaks. These features may be explained as the result of the large magnetic coupling between the two transmitting resonators. In the DTR-WPT system, the two transmitting resonators form a parasitic STR-WPT system with no load resistance. Therefore, if the effect of the receiving resonator on $i_1$ is assumed to be small, the comparatively large magnetic coupling between the two transmitting coils can explain two peaks in the frequency dependency of $i_1$, which is natural in the STR-WPT system with no load resistance [4].

**3.2 Verification of the Output Power and the Optimum Load Impedance** Next, the optimum load impedance for maximizing the output power was experimentally evaluated; and the result was compared with the theoretical prediction. As discussed in subsection 2.2, optimization

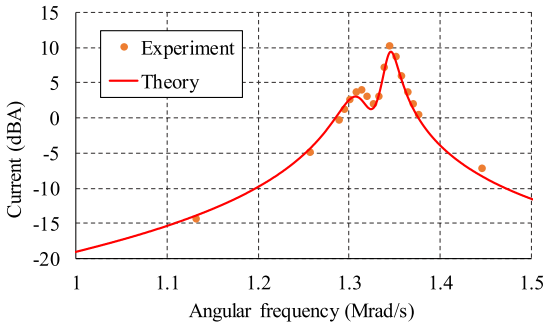


(a) Amplitude of current $i_1$ of transmitting coil W1.

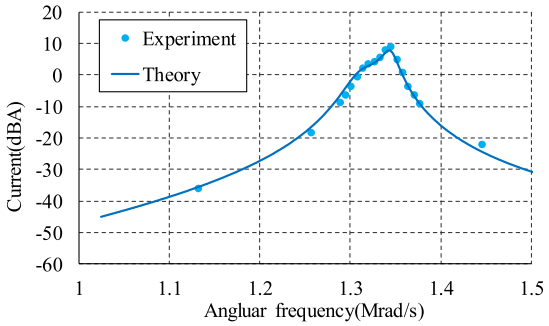


(b) Amplitude of current $i_2$ of transmitting coil W2.

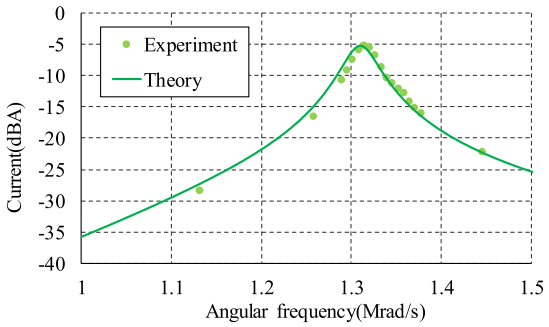


(c) Amplitude of current $i_3$ of receiving coil W3.

Fig. 10. Frequency dependency of experimental current amplitude near the resonance angular frequency

of the load impedance to maximize the output power also requires optimization of the angular frequency. Therefore, we first confirmed the appropriateness of the optimum angular frequency for maximizing the output power under a given load impedance, which can be predicted according to (17).

For this purpose, we measured the frequency dependency of the load current amplitude under the load impedance of 10 Ω. The AC voltage applied to the transmitting resonator A was set to have the amplitude of 10.0 Vp-p. The output power is calculated based on the resistance of the load and the square of the effective value of the load current.

Figure 11 shows the result near the resonant frequency. As can be seen in this figure, the frequency dependency of the output power well agreed with the theory, i.e. (17). According to the experimental result, the peak output power was observed at the angular frequency of 1.313 Mrad/s. On the other hand, the theory predicted the peak output power at 1.310 Mrad/s. Therefore, the result supported the appropriateness of the theory in predicting the optimum angular frequency.

Next, we searched for the optimum angular frequency and evaluated the output power at this angular frequency, i.e. the peak output power, for various values of the load impedance.

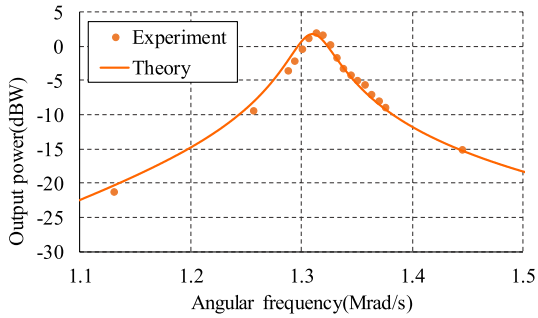


Fig. 11. Frequency dependency of the output power under the load resistance of 10 Ω

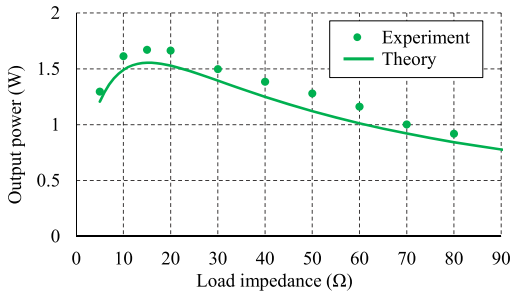


Fig. 12. Dependency of the output power on the load resistance. The angular frequency was optimized so that the output power was maximized at each value of the load resistance

The load impedance was ranged from 5 Ω to 80 Ω. The AC voltage applied to the transmitting resonator A was set to have the amplitude of 10.0 Vp-p. Then, the result was compared with the theoretical prediction based on (17). Theoretical prediction of the peak output power was performed by numerically searching for the maximum of the right-hand side of (17) under a given load impedance.

Figure 12 shows the relation between the peak output power and the load impedance. The overall feature of the load impedance dependency of the peak output power well agreed between the experiment and the theory. Certainly, the experimental result of the output power was slightly higher than the theoretical prediction. However, compared with prediction of the current, prediction of the output power tends to have large error because the output power is calculated based on the square of the current amplitude of the load. In fact, the deviation between the experiment and the theory in Fig. 12 indicates that the theory predicted the amplitude of the load current within an error of 6.6%. Therefore, the experimental result in Fig. 12 well agreed with the theoretical prediction, supporting appropriateness of (17).

The peak of the experimental result in Fig. 12 appeared at the load impedance of 15 Ω. Therefore, the optimum load impedance was evaluated as 15 Ω approximately. This value is also consistent with the theory because the optimum load impedance was predicted as 15.3 Ω according to the proposed method based on (22).

Consequently, the experiment supported appropriateness of the proposed method to derive the optimum load impedance.

## 4. Conclusions

Resonant inductive coupling WPT systems for small mobile apparatus tend to suffer from low power transfer

capability due to weak magnetic coupling between the transmitting and receiving resonators. Recently, the DTR-WPT has been proposed as an attractive technique that can improve the power transfer capability to a distant place. However, elucidation of the design optimization method for the DTR-WPT is generally difficult because of complicated magnetic coupling among its two transmitting resonators and one receiving resonator, hindering practical application of this technique to industry.

This paper addressed this issue by proposing a design optimization method of the load impedance, which can be adjusted using the power conversion techniques. This paper derived a simplified equivalent circuit model of the DTR-WPT system. Then, the optimum load resistance was derived based on the analysis of this model.

Experiment was carried out to verify the proposed method. The result showed good agreement with the analysis of the simplified equivalent circuit model. Furthermore, the experiment revealed that the optimum load resistance was successfully predicted by the proposed method.

Consequently, we concluded that the proposed method is promising for design optimization of the load resistance for the DTR-WPT system.

## References


(1) Z.N. Low, R.A. Chinga, and R. Tseng: "Design and test of a high-power high-efficiency loosely coupled planar wireless power transfer system", *IEEE Trans. Ind. Electron*., Vol.56, No.5, pp1801–1812 (2009)

(2) T. Imura and Y. Hori: "Maximizing air gap and efficiency of magnetic resonant coupling for wireless power transfer using equivalent circuit and Neumann formula", *IEEE Trans. Ind. Electron*., Vol.58, No.10, pp.4746–4752 (2011)

(3) R. Bosshard, J. Muhlethaler, J.W. Kolar, and I. Stevanovic: "Optimized magnetic design for inductive power transfer coils", Proc. IEEE Appl. Power Electron. Conf. Expo. (APEC), pp.1812–1819 (2013)

(4) I. Awai: "Basic characteristics of "Magnetic resonance" Wireless Power Transfer System Excited by a 0 Ohm Power Source", *IEICE Electron. Express*, Vol.10, No.21, pp.1–13 (2013)

(5) R. Huang, B. Zhang, D. Qiu, and Y. Zhang: "Frequency splitting phenomena of magnetic resonant coupling wireless power transfer", *IEEE Trans. Magn*., Vol.50, No.11, 8600204 (2014)

(6) D. Ahn and S. Hong: "Wireless power transfer resonance coupling amplification by load-modulation switching controller", *IEEE Trans. Ind. Electron*., Vol.62, No.2, pp.898–909 (2015)

(7) V. Jiwariyavej, T. Imura, and Y. Hori: "Coupling coefficients estimation of wireless power transfer system via magnetic resonance coupling using information from either side of the system", *IEEE J. Emerg. Sel. Topics Power Electron*., Vol.3, No.1, pp.191–200 (2015)

(8) H. Li, J. Li, K. Wang, W. Chen, and X. Yang: "A maximum efficiency point tracking control scheme for wireless power transfer systems using magnetic resonant coupling", *IEEE Trans. Power Electron*., Vol.30, No.7, pp.3998–4008 (2015)

(9) M.R.V. Moghadam and R. Zhang: "Multiuser wireless power transfer via magnetic resonant coupling: performance analysis, charging control, and power region characterization", *IEEE Trans. Signal Inform. Process. Over Networks*, Vol.2, No.1, pp.72–82 (2016)

(10) T.V. Nguyen, H.S. Kang, H.J. Choi, and W.C. Jung: "Magnetic resonance wireless power transfer using three-coil system with single planar receiver for laptop applications", *IEEE Trans. Consumer Electron*., Vol.61, No.2, pp.160–166 (2015)

(11) H. Jiang, J. Zhang, D. Lan, K.K. Chao, S. Liou, H. Shahnasser, R. Fechter, S. Hirose, M. Harrison, and S. Roy: "A low-frequency versatile wireless power transfer technology for biomedical implants", *IEEE Trans. Biomed. Circuits Syst*., Vol.7, No.4, pp.526–535 (2013)

(12) R. Xue, K. Cheng, and M. Je: "High-efficiency wireless power transfer for biomedical implants by optimal resonant load transformation", *IEEE Trans. Circuits Syst. I, Reg. Papers*, Vol.60, No.4, pp.867–874 (2013)

(13) K.A. RamRakhyani and G. Lazzi: "On the design of efficient multi-coil telemetry system for biomedical implants", *IEEE Trans. Biomed. Circuits Syst*., Vol.7, No.1, pp.11–23 (2013)

(14) H. Liu, Q. Shao, and X. Fang: "Modeling and optimization of class-E amplifier at subnominal condition in a wireless power transfer system for biomedical implants", *IEEE Trans. Biomed. Circuits Syst*., Vol.PP, No.99, pp.1–9 (2016)

(15) S. Li and C.C. Mi: "Wireless power transfer for electric vehicle applications", *IEEE Trans. Emerg. Sel. Topics Power Electron*., Vol.3, No.1, pp.4–17 (2015)

(16) M.J. Miller, C.O. Onar, and M. Chinthavali: "Primary-side power flow control of wireless power transfer for electric vehicle charging", *IEEE Trans. Emerg. Sel. Topics Power Electron*., Vol.3, No.1, pp.147–162 (2015)

(17) C.C. Mi, G. Buja, Y.S. Choi, and T.C. Rim: "Modern advances in wireless power transfer systems for roadway powered electric vehicles", *IEEE Trans. Ind. Electron*., Vol.63, No.10, pp.6533–6545 (2016)

(18) G. Buja, M. Bertoluzzo, and K.N. Mude: "Design and experimentation of WPT charger for electric city car", *IEEE Trans. Ind. Electron*., Vol.62, No.12, pp.7436–7447 (2015)

(19) H. Kim, C. Song, D.-H. Kim, D.H. Jung, I.-M. Kim, Y.-I. Kim, J. Kim, S. Ahn, and J. Kim: "Coil design and measurements of automotive magnetic resonant wireless charging systems for high-efficiency and low magnetic field leakage", *IEEE Trans. Mirow. Theory Techn*., Vol.64, No.2, pp.383–400 (2016)

(20) R. Itoh, Y. Sawahara, T. Ishizaki, and I. Awai: "Construction of secure wireless power transfer system for robot fish", Proc. IEEE Wireless Power Transfer Conf., F3.6, pp.1–4 (2015)

(21) M.Q. Nguyen, Y. Chou, D. Plesa, S. Rao, and J.C. Chiao: "Multiple-inputs and multiple-outputs wireless power combining and delivering systems", *IEEE Trans. Power Electron*., Vol.30, No.11, pp.6254–6263 (2015)

(22) K.E. Koh, K. Song, P. Sukprasert, T. Imura, and Y. Hori: "Two-transmitter wireless power transfer with LCLcircuit for continuous power in dynamic charging", Proc. 2015 IEEE PELS Workshop Emerg. Techn., Wireless Power (WoW) (2015)

**Takahiro Koyama** (Student Member) received the B. degree in electrical engineering from Okayama University, Okayama, Japan in 2015. He is currently a student of Graduate School of Natural Science and Technology, Okayama University, Japan. His research interest includes magnetic analysis for wireless power transfer. He is a student member of the Institute of Electrical and Electronics Engineers.

**Kazuhiro Umetani** (Member) was born in Kobe, Japan. He received the M. and Ph.D. degree in geophysical fluid dynamics from Kyoto University, Kyoto, Japan in 2004 and 2007, respectively. In 2015, he received the second Ph.D. degree in electrical engineering from Shimane University, Japan. From 2007 to 2008, he was a Circuit Design Engineer for Toshiba Corporation, Japan. From 2008 to 2014, he was with the Power Electronics Group in DENSO CORPORATION, Japan. He is currently an Assistant Professor at Okayama University, Okayama, Japan. His research interests include new circuit configurations in power electronics and power magnetics for vehicular applications. Dr. Umetani is a member of the Institute of Electrical and Electronics Engineers and the Japan Institute of Power Electronics.

**Eiji Hiraki** (Member) received the M.Sc. and Ph.D. degrees from Osaka University, Osaka, Japan, in 1990 and 2004, respectively. He joined Mazda Motor Corporation in 1990. From 1995 to 2013, he was with the Power Electronics Laboratory, Yamaguchi University, Yamaguchi, Japan. He is currently a Professor with the Electric Power Conversion System Engineering Laboratory, Okayama University, Okayama, Japan. His research interests include circuits and control systems of power electronics, particularly soft-switching technique for high-frequency switching power conversion systems. Dr. Hiraki is a member of the Institute of Electrical Engineers of Japan and the Japan Institute of Power Electronics.